Check for updates

Received: 2 August 2023 | Revised: 20 December 2023 | Accepted: 10 January 2024

DOI: 10.1002/mawe.202300164

ARTICLE

WILEY VCH

Use of a low transformation temperature effect for the targeted reduction of welding distortion in stainless chromium-nickel steel for an application in rail vehicle construction

Nutzung eines Niedrigtransformationstemperatureffektes zur gezielten Reduzierung von Schweißverzug in korrosionsbeständigem Chrom-Nickel-Stahl für die Anwendung im Schienenfahrzeugbau

M. Gamerdinger[1] | F. Akyel[1] | S. Olschok[1] | C. Kahve[2] | D. C. Fritsche[2] | U. Elliesen[3] | C. Hopmann[2] | U. Reisgen[1]

[1]Welding and Joining Institute
RWTH Aachen University
Aachen, Germany

[2]Institute for Plastics Processing (IKV) in Industry and Craft
RWTH Aachen University
Aachen, Germany

[3]Photon Laser Manufacturing GmbH
Berlin, Germany

Correspondence
M. Gamerdinger, Welding and Joining Institute RWTH Aachen University
52062 Aachen, Germany.
Email:
max.gamerdinger@isf.rwth-aachen.de

Abstract

Due to their low thermal conductivity and high thermal expansion, austenitic chromium-nickel steels have an increased tendency to distortion during welding. In industrial sectors such as rail vehicle construction, there is a high demand for geometrical precision that is not met by distorted components. Introducing a low transformation temperature (LTT) effect in the weld seam influences the stress distribution, which effects the formation of welding distortion. The low transformation temperature effect is achieved by in situ alloying using commercially available materials. The demonstrators made of stainless steel (X2CrNiN18-7/1.4318) were welded with a low-alloy filler metal G4Si1. The low transformation temperature effect is assessed by energy dispersive x-ray spectroscopy and hardness measurements. The effect on distortion was investigated by measuring the demonstrators with a coordinate measuring system and the results were compared with the reference stainless steel demonstrators with stainless filler metal. The alloying process resulted in a reduction of the alloy content to 14.4 m% chromium and 5 m% nickel and a medium-high hardness of 361 HV 0.2 to 383 HV 0.2. The low transformation temperature effect achieved leads to a significant reduction in welding distortion of up to 78% compared to the similar reference demonstrators.

This is an open access article under the terms of the Creative Commons Attribution-NonCommercial-NoDerivs License, which permits use and distribution in any medium, provided the original work is properly cited, the use is non-commercial and no modifications or adaptations are made.
© 2024 The Author(s). *Materialwiss. Werkstofftech.* published by Wiley-VCH GmbH.

KEYWORDS
dissimilar welding components, laser beam welding, low transformation temperature (LTT), rail vehicle construction, welding distortion

Abstract

Austenitische Chrom-Nickel Stähle neigen aufgrund ihrer geringen Wärmeleitfähigkeit und hohen Wärmeausdehnung verstärkt zum Verzug beim Schweißen. In Industriezweigen wie dem Schienenfahrzeugbau werden hohe Anforderungen an die geometrische Präzision gestellt, die durch verzogene Bauteile nicht erfüllt werden. Das Einbringen eines Niedrigtransformationstemperatureffektes (LTT) in die Schweißnaht beeinflusst die Spannungsverteilung, was sich auf die Entstehung von Schweißverzug auswirkt. Der Niedrigtransformationstemperatureffektes wird durch in situ Legieren mit handelsüblichen Werkstoffen erreicht. Die Demonstratoren aus nichtrostendem Stahl (X2CrNiN18-7/1.4318) wurden mit einem niedriglegierten Schweißzusatzwerkstoff G4Si1 verschweißt. Der Niedrigtransformationstemperatureffektes wird durch energiedispersive Röntgenspektroskopie und Härtemessungen beurteilt. Der Einfluss auf den Verzug wurde durch Vermessung der Demonstratoren mit einem Koordinatenmesssystem untersucht und die Ergebnisse mit den Referenzdemonstratoren aus nichtrostendem Stahl geschweißt mit nichtrostendem Schweißzusatz verglichen. Durch den Legierungsprozess wurde eine Reduzierung des Legierungsgehalt auf 14.4 m% Chrom und 5 m% Nickel und eine mittelhohe Härte von 361 HV 0.1 bis 383 HV 0.1 erreicht. Der erzielte Niedrigtransformationstemperatureffektes führt zu einer signifikanten Reduzierung des Schweißverzugs von bis zu 78 % im Vergleich zu den artgleichen Referenzdemonstratoren.

SCHLÜSSELWÖRTER
artfremde Schweißverbindung, Laserstrahlschweißen, Niedrigtransformationstemperatureffekt (LTT), Schienenfahrzeugbau, Schweißverzug

1 | INTRODUCTION

The local heat input during the welding process leads to inhomogeneous temperature distribution. During the cooling of the sample, the shrinkage of the weld material is restricted by the surrounding cooler material. This inevitably leads to inhomogeneous stress distribution and in the end to tensile residual stresses within the weldment [1–3]. The stress builds up during cooling to the point, where the temperature dependent yield stress is reached [4, 5]. If the stress within the weld exceeds the yield stress, elastic compensation cannot be achieved anymore and the result is plastic deformation. This distortion can be divided into two typical categories. A distinction is made between in-plane and out-of-plane distortion. The in-plane distortions are longitudinal and transverse as well as rotational shrinkage. In the case of out-of-plane distortions, a distinction is made between angular distortion, buckling and longitudinal bending [6]. Panel structures made of thin sheet metal ($t < 4$ mm) with longitudinal and transverse stiffeners are a typical welding task in rail vehicle construction. This structure leads to a complex combination of distortion due to the welding of the individual seams. As a result, the angular distortion from all seams leads to inward buckling in the center of the panel [7]. Distortion can be affected and reduced by various methods, such as adapted design of the component, control of heat input, amount of tack welds, restraint, welding sequence or active mitigation techniques [8–11]. However, for some products, it is not possible to redesign the components with a design adapted to the welding process or to change the welding sequence. In such cases, a targeted adjustment of the heat input is a suitable mitigation technique. Nevertheless, even joining processes with low heat input such as laser beam welding can lead to a high degree of welding distortion

15214052, 2024, 7, Downloaded from https://onlinelibrary.wiley.com/doi/10.1002/mawe.202300164 by Rwth Aachen, Wiley Online Library on [12/12/2024]. See the Terms and Conditions (https://onlinelibrary.wiley.com/terms-and-conditions) on Wiley Online Library for rules of use; OA articles are governed by the applicable Creative Commons License

in complex components such as structural panels. In these cases, a preventive strategy to avoid the development of distortion by specifically influencing residual welding stresses can be particularly useful.

Two factors need to be taken into account when describing welding residual stresses: thermal shrinkage due to the described local heat input (tensile stresses are introduced) and phase transformations (compressive stresses are introduced). While the transformation of austenite into ferrite leads to volume expansion, the compressive stresses can only build up to the temperature-dependent yield point and are thus reduced in effect. However, the greatest volume expansion and the highest build-up of compressive stresses can be achieved with a martensitic phase transformation, as here the yield strength is no longer necessarily limiting [1]. It is known that the volume expansion increases, if the martensite start temperature is reduced up to the point where the martensite finish temperature is reached [12–16]. Since the martensite start temperature can be easily manipulated by the chemical composition, it is an important control variable for setting the stress state. First studies about this so-called low transformation temperature (LTT) effect showed promising results regarding residual stress reduction and thus also welding distortion [5,14]. Further studies have been performed, where various filler materials were analysed [12,16–19]. However, all these studies where performed in arc welding and mostly in mild steel with specifically designed filler materials. Previous studies by the authors have shown that the low transformation temperature effect can also be used with dissimilar material combinations in stainless steel with the use of commonly available weld consumables in laser and electron beam welding [20–22]. Especially the results in 2 mm thin sheets showed promising results in avoidance of distortion [22]. In modern rail vehicles, stainless steels are increasingly being used for lightweight construction due to their high strength and good corrosion resistance. However, due to their high thermal expansion and low thermal conductivity, austenitic stainless steels are prone to distortion during welding [23]. Particularly in the case of long, flat and complex components, the distortion leads to inadmissible dimensional and shape deviations, which have to be eliminated at great expense by straightening work. It is therefore important to avoid welding distortion in its development.

In the past, the focus was on demonstrating the low transformation temperature effect by means of simple bead-on-plate welds when using an in situ alloyed low transformation temperature effect for laser beam welding with commercially available and industry-typical welding consumables. To date, no work has been carried out to apply this in situ low transformation temperature effect in a practical application. The aim of the present work is to further develop this welding process from a simple bead-on-plate to its use in an industrially comparable welding task. The welding tasks are demonstrators that represent a section of a panel structure with several weld seams. The aim is to investigate and demonstrate how the resulting low transformation temperature effect can be used to reduce welding distortion.

2 | METHODS

In total, 12 demonstrators were welded. The welding process for the similar reference demonstrators, thus the material combination and welding sequence used, were provided by photon laser manufacturing GmbH. This welding process represent a typical welding task for a section of a panel structure from the outer skin area of a rail vehicle, Figure 1. The base material of the demonstrators was a high alloy chrome-nickel steel 1.4318 (X2CrNiN18-7/ASTM 301LN) provided by Outokumpu Nirosta GmbH. Two different filler wires were added to the weld seam for the in situ alloying process. For the similar reference demonstrators, a high alloy filler wire G19 9 (EN ISO 14343-A: G19 9 L Si) was used. To obtain the low transformation temperature effect in the demonstrators, the chemical composition must be reduced. A commercially available low alloy filler wire is required for the in situ alloying process. A G4Si1 (EN ISO 14341 A: G 42 2 C1 4Si1), which is commonly available in the industry, was therefore used and the low transformation temperature effect was set by diluting the base material with it. Both filler wires had a diameter of 1 mm. Argon 4.8 (DIN EN ISO 14175-I1-Ar) was fed into the process as the shielding gas. The chemical composition of the base materials and filler wires were measured by optical emission spectroscopy (OES), Table 1. The demonstrators consist of a base sheet 400 mm×400 mm×2.0 mm onto which two ribs each measuring 400 mm×50 mm×3.0 mm and 300 mm×50 mm×3.0 mm are welded, Figure 1a. A total of 12 weld seams from S1 to S12 are welded each demonstrator. First the long ribs are tack welded with tungsten inert gas welding and then laser welded from seam S1 to S4, then the short ribs are tack welded and then welded with seams S5 to S12, Figure 1b. Welding direction of the short ribs is from the outside to the center with an overlap of 10 mm of the seams welded towards each other. The seam in the overlap area are named after the two connecting seams, for example, overlap between S5 and S9 is named S5;9. The wire is positioned at 45° to

15214052, 2024, 7, Downloaded from https://onlinelibrary.wiley.com/doi/10.1002/mawe.202300164 by Rwth Aachen, Wiley Online Library on [12/12/2024]. See the Terms and Conditions (https://onlinelibrary.wiley.com/terms-and-conditions) on Wiley Online Library for rules of use; OA articles are governed by the applicable Creative Commons License

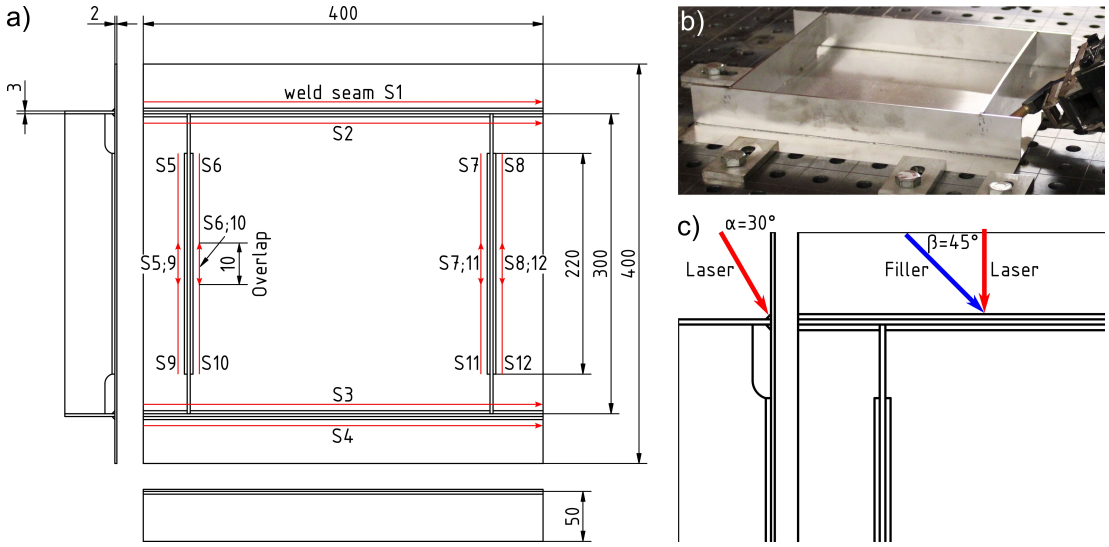


FIGURE 1 Geometric relationships in the welding trials. Subfigure a) shows the dimensions of the demonstrators as well as the position of the welds S1 to S12. Subfigure b) shows a demonstrator before welding the seams S5 to S12 and c) shows the angular correlations between laser, specimen and filler wire.

BILD 1 Geometrische Verhältnisse bei den Schweißversuchen. Teilbild a) zeigt die Abmessungen der Demonstratoren sowie die Lage der Schweißnähte S1 bis S12. Teilbild b) zeigt einen Demonstrator vor dem Schweißen der Nähte S5 bis S12 und c) zeigt die Winkelbeziehungen zwischen Laserstrahl, Probe und Zusatzdraht.

TABLE 1 Chemical composition measured by optical emission spectroscopy

TABELLE 1 Chemische Zusammensetzung gemessen mittels optischer Emissionsspektroskopie

	Alloying elements [m%]					
Material	**Carbon**	**Chromium**	**Nickel**	**Molybdenum**	**Manganese**	**Silicon**
1.4318, 3.0 mm	0.038	17.49	6.42	0.159	1.197	0.46
1.4318, 2.0 mm	0.034	17.70	6.387	0.073	1.19	0.416
G 19 9 L Si	0.025	19.72	10.14	0.156	1.71	0.734
G4Si1	0.107	0.031	0.015	0.0030	1.74	0.977

the laser in a trailing arrangement and laser/wire at 30° to the specimen, Figure 1c.

Welding was carried out with a Trumpf TruDisk 8002 laser with a wavelength of 1030 nm and a Scansonic ALO3 optics. The same welding parameters were used for all weld seams and both alloy combinations in order to obtain a comparable seam formation, Table 2. For each alloy composition, 6 demonstrators were welded. The metallurgical and chemical investigations such as cross-sections (etched with V2 A stain, DIN EN ISO 17639:2022), Vickers hardness test (DIN EN ISO 9015-2) and chemical analyses were carried out on the 12 weld seams of one of the demonstrators and the distortion

TABLE 2 Information on the equipment and welding parameters

TABELLE 2 Informationen zum Equipment und den Schweißparameter

Laser:	**Trumpf TruDisk 8002**		
Optic	**Scansonic ALO3**	**Welding parameters:**	
Fiber diameter [µm]	600	Power P [W]	2200
Aspect ratio	1:1.6	Welding speed v_w [mm/s]	28
Focal length [mm]	176	Feeding speed v_f [mm/s]	25
spot diameter [µm]	960	Shielding gas flow [l/min]	20

15214052, 2024, 7, Downloaded from https://onlinelibrary.wiley.com/doi/10.1002/mawe.202300164 by Rwth Aachen, Wiley Online Library on [12/12/2024]. See the Terms and Conditions (https://onlinelibrary.wiley.com/terms-and-conditions) on Wiley Online Library for rules of use; OA articles are governed by the applicable Creative Commons License

measurements were carried out on the remaining 5 demonstrators [24, 25].

3 | RESULTS

3.1 | Cross sections

For the examination of the welding results, transverse sections were first prepared, Figure 2. The analysis is carried out on three representative sections. From the long ribs weld seam S1/S2, from the short ribs weld seam S5/S6 and from the overlap area weld seams S5;9/S6;10.

Each transverse section shows two welds. By setting the laser and the wire at 30°, the weld seam forms more strongly in the 3.0 mm sheet. The aim is a full connection of the web plate by a weld seam on each side. A slightly variable formation of the weld seams can be seen in all transverse sections. The seam S5;9 shows several melt lines in the low transformation temperature demonstrator, which is due to the double melting by the two seams S5 and S9. The variation of the seams as well as the double melting zones in the overlap can be attributed to a tolerable mispositioning due to the fully automatic welding process. Overall, however, no impermissible welding irregularities can be seen in the weld seams. In addition to the cross-sections, no significant irregularities can be detected in the top view of the resulting weld seams, Figure 2.

3.2 | Hardness

Since the low transformation temperature effect is based on a martensitic phase transformation, the presence of the effect can be investigated by hardness measurements and examination of the chemical composition. Hardness measurements were carried out on the welds S1 and S2, Figure 3. Measurements were taken on measuring lines along the longitudinal axis (C, D) and transverse to the seam (A, B), Figure 4b. For the low transformation temperature welds, the base material shows a low hardness (about 210 HV 0.2). The first measuring points in the seam are reached at 1.4 mm (A) and 1.6 mm (B) and the hardness jumps to high values of about 375 HV 0.2, Figure 3a.

In the measurements across the weld, the hardness of the seam S1 drops sharply along the measuring line C until the base material or the heat affected zone is reached at 3.4 mm, Figure 3b. This behaviour does not occur with the seam S2 line D. Here, the hardness values remain at the higher values until the heat affected zone or base material is reached. Basically, however, weld S2 shows a slightly lower hardness at a more constant hardness level than weld S1, Figure 4a. The reason for this could be the locally increased specimen temperature due to the welding of seam S1, which leads to a slower cooling rate of seam S2. On the other hand, the drop in hardness of seam S1 (C) can be attributed to the heat effect caused by the welding of seam S2. By reheating, a kind of tempering treatment takes place, which reduces the hardness in the root of S1. No significant increase in hardness can be observed for the similar weld seams. Since the base material is a high alloy austenitic chromium-nickel steel, no hardening is possible due to the

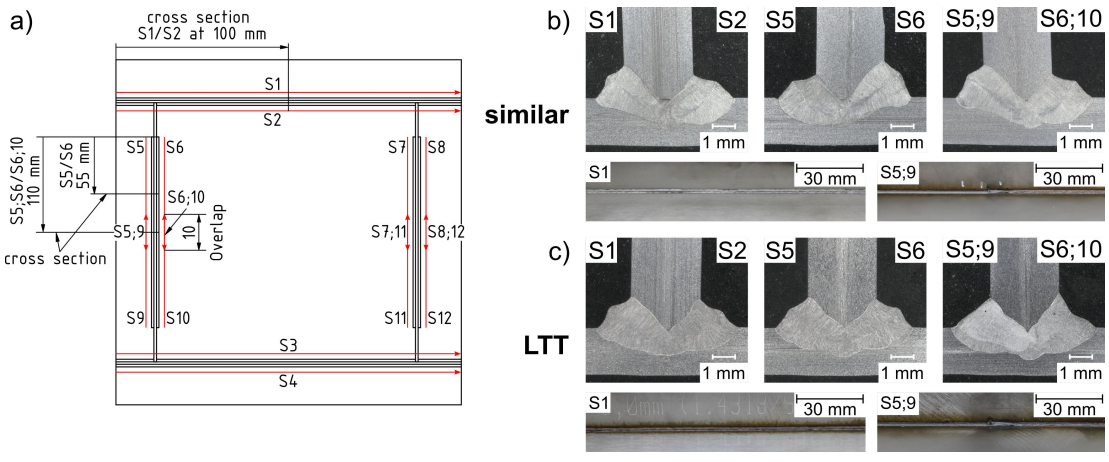


FIGURE 2 Overview of the removal positions of the cross-sections in section a). Top view of the weld seams S1 and S5;S9 and cross-sections for the similar demonstrators b) and for the low transformation temperature demonstrators c).

BILD 2 Übersicht über die Entnahmepositionen der Querschliffe in Teilbild a). Draufsicht der Schweißnähte S1 und S5;S9 und Querschliffe für die artgleichen Demonstratoren b) und für die Niedrigtransformationstemperatur Demonstratoren c).

15214052, 2024, 7, Downloaded from https://onlinelibrary.wiley.com/doi/10.1002/mawe.202300164 by Rwth Aachen, Wiley Online Library on [12/12/2024]. See the Terms and Conditions (https://onlinelibrary.wiley.com/terms-and-conditions) on Wiley Online Library for rules of use; OA articles are governed by the applicable Creative Commons License

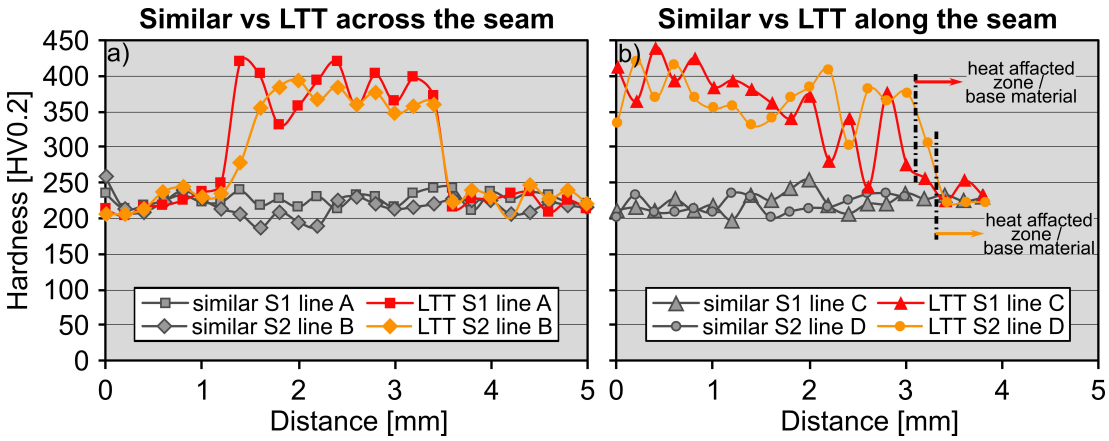


FIGURE 3 Hardness curve of the weld seams. Subfigure a) shows the curve transverse to the weld seam and subfigure b) shows the curve along the longitudinal axis.

BILD 3 Härteverlauf der Schweißnähte. In Teilbild a) ist der Verlauf quer zur Schweißnaht und in Teilbild b) der Verlauf entlang der Längsachse aufgetragen.

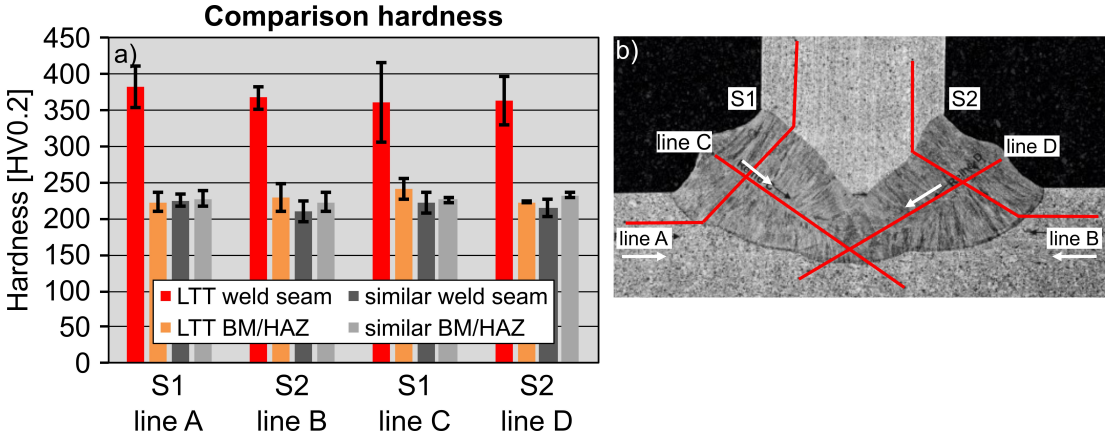


FIGURE 4 Comparison of the hardness values of the similar and the low transformation temperature welds for the areas of the weld and the base material/heat affected zone. Subfigure b) shows the position of the measured hardness lines.

BILD 4 Vergleich der Härtewerte der artgleichen und der Niedrigtransformationstemperatur-Schweißnähte für die Bereiche der Schweißnaht und der Grundwerkstoff/Wärmeeinflusszone. Teilbild b) zeigt die Lage der gemessenen Härtelinien.

absence of the transformation from face-centred cubic to body-centered cubic.

As described, the hardness measurements in the head of S1 shows higher values than the seam S2, but also a higher variation, Figure 4a. The drop in hardness of weld S1 along measurement line C is mainly reflected in the lower mean value and the larger error bar. Low hardness values can be seen both for the welds and for the heat affected zone and base material of the similar specimen, Table 3. The increased hardness of the low transformation temperature seams is an indicator for martensitic welds and are in good agreement with values for alloys with a low transformation temperature effect and the author's own preliminary work [19–21, 26].

3.3 | Chemical composition

The martensite start temperature serves as an important control variable for the low transformation temperature effect and can be influenced by varying the chemical composition. To investigate the alloy content, line scans were performed along the longitudinal axis of the welds using energy dispersive x-ray spectroscopy (EDS). A comprehensive chemical composition study was carried out on all welds of the low transformation temperature demonstrator, Table 4. For a direct comparison of the chemical composition, the course of the chromium and nickel content was plotted over the longitudinal axis of the weld, Figure 5. The progressions from the seams S1 and S2 as well as the seams from the overlap area S5; 9 and S6; 10 are shown. The chromium content is plotted

15214052, 2024, 7, Downloaded from https://onlinelibrary.wiley.com/doi/10.1002/mawe.202300164 by Rwth Aachen, Wiley Online Library on [12/12/2024]. See the Terms and Conditions (https://onlinelibrary.wiley.com/terms-and-conditions) on Wiley Online Library for rules of use; OA articles are governed by the applicable Creative Commons License

TABLE 3 Mean values and standard deviation of hardness

TABELLE 3 Mittelwerte und Standardabweichung der Härte

			similar		low transformation temperature (LTT)	
		line	Weld seam	Heat affected zone/ base material	Weld seam	Heat affected zone/ base material
Hardness [HV0.2]	S1	A	225.3 ± 8.5	227.8 ± 10	383.0 ± 28.8	223 ± 12.4
		C	222.3 ± 13.7	226.5 ± 3.5	360.8 ± 54.5	241.3 ± 15.5
	S2	B	209.3 ± 14.5	222.3 ± 13.1	367.8 ± 15.5	229.1 ± 18.8
		D	215.3 ± 11.6	232.7 ± 3.2	362.8 ± 34	223.33 ± 0.58

TABLE 4 Chemical composition measured by energy dispersive x-ray spectroscopy and calculated carbon content as well as martensite start temperature (M_s).

TABELLE 4 Mittels energiedispersiver Röntgenspektroskopie gemessene chemische Zusammensetzung und berechneter Kohlenstoff Gehalt sowie Martensitstarttemperatur (M_s).

	Chemical composition [m%]					Ratio		Carbon by (2)–(4)	
LTT	Chromium	Nickel	Molybdenum	Manganese	Silicon	xBM	xFW	[m%]	Ms by (1)
S1	14.48 ± 0.52	5.08 ± 0.28	0.15 ± 0.06	0.98 ± 0.14	0.52 ± 0.07	0.8276	0.1724	0.0503	169
S2	14.40 ± 0.40	5.02 ± 0.30	0.16 ± 0.07	0.93 ± 0.12	0.52 ± 0.06	0.823	0.177	0.0506	173
S3	14.39 ± 0.58	4.95 ± 0.31	0.16 ± 0.08	0.94 ± 0.10	0.49 ± 0.05	0.8224	0.1776	0.0506	174
S4	14.55 ± 0.50	5.05 ± 0.24	0.17 ± 0.06	0.95 ± 0.11	0.5 ± 0.06	0.8316	0.1684	0.05	169
S5	14.41 ± 0.64	5.06 ± 0.24	0.16 ± 0.07	0.96 ± 0.10	0.52 ± 0.06	0.8236	0.1764	0.0506	171
S6	14.30 ± 0.51	5.03 ± 0.21	0.15 ± 0.07	0.94 ± 0.09	0.52 ± 0.05	0.8173	0.1827	0.051	174
S7	14.35 ± 0.49	4.98 ± 0.25	0.15 ± 0.07	0.95 ± 0.13	0.52 ± 0.07	0.8201	0.1799	0.0508	174
S8	14.32 ± 0.52	4.94 ± 0.23	0.16 ± 0.08	0.92 ± 0.14	0.50 ± 0.06	0.8184	0.1816	0.0509	176
S9	14.42 ± 0.56	5.00 ± 0.26	0.17 ± 0.08	0.95 ± 0.13	0.53 ± 0.07	0.8242	0.1758	0.0505	172
S10	14.39 ± 0.46	5.01 ± 0.31	0.18 ± 0.08	0.93 ± 0.12	0.48 ± 0.06	0.8224	0.1776	0.0506	173
S11	14.55 ± 0.86	5.09 ± 0.33	0.15 ± 0.07	0.96 ± 0.10	0.49 ± 0.05	0.8316	0.1684	0.05	169
S12	14.34 ± 0.45	5.02 ± 0.19	0.18 ± 0.10	0.96 ± 0.12	0.49 ± 0.06	0.8196	0.1804	0.0508	172
S5;9	12.71 ± 1.52	4.61 ± 0.60	0.17 ± 0.09	0.94 ± 0.13	0.53 ± 0.08	0.7262	0.2738	0.0573	205
S6;10	12.77 ± 1.05	4.59 ± 0.44	0.17 ± 0.09	0.92 ± 0.15	0.55 ± 0.06	0.7297	0.2703	0.057	205
S7;11	12.79 ± 1.41	4.74 ± 0.65	0.19 ± 0.11	1.18 ± 0.26	0.49 ± 0.08	0.7308	0.2692	0.0569	193
S8;12	12.71 ± 1.45	4.63 ± 0.71	0.19 ± 0.11	1.23 ± 0.28	0.46 ± 0.1	0.7262	0.2738	0.0573	194

on the left side, Figure 5a. For reference, the chromium content of the similar demonstrator seam S1 is plotted as a dashed line. Since the joint is a similar material combination (1.4318 + G19 9), no significant fluctuations in the alloy content can be detected.

For the low transformation temperature demonstrator, the chromium content is reduced by alloying with G4Si1. For the welds S1 and S2 (red, orange), an alloy content of about 14.4 m% chromium is found in the weld without major fluctuations. When the base metal is reached, the alloy content jumps to the initial level. However, if the chromium content from S1 and S2 is compared with that from seams S5;9 and S6;10, there are clear differences. Since the welds S5;9 and S6;10 are in the overlap area, they are welded over twice and therefore more unalloyed filler metal is introduced. This results in a greater reduction in the alloy content to 12.7 m% of chromium. Considering the course of the nickel content, a similar pattern can be observed, Figure 5b. The differences in alloy content between the seams S1 and S2 (about 5 m%) and S5;9 and S6;10 (about 4.6 m%) are not so clearly visible.

In all seams of the low transformation temperature demonstrator S1 to S12 a uniform alloy content is established without being subject to large fluctuations, Figure 6. The observed behavior of the overlap areas S5;9 and S6;10 also occurs in the other two overlap areas S7;11 and S8;12. This results in two different alloy areas in the demonstrators with low transformation temperature effect. By knowing the alloy content, the resulting

15214052, 2024, 7, Downloaded from https://onlinelibrary.wiley.com/doi/10.1002/mawe.202300164 by Rwth Aachen, Wiley Online Library on [12/12/2024]. See the Terms and Conditions (https://onlinelibrary.wiley.com/terms-and-conditions) on Wiley Online Library for rules of use; OA articles are governed by the applicable Creative Commons License

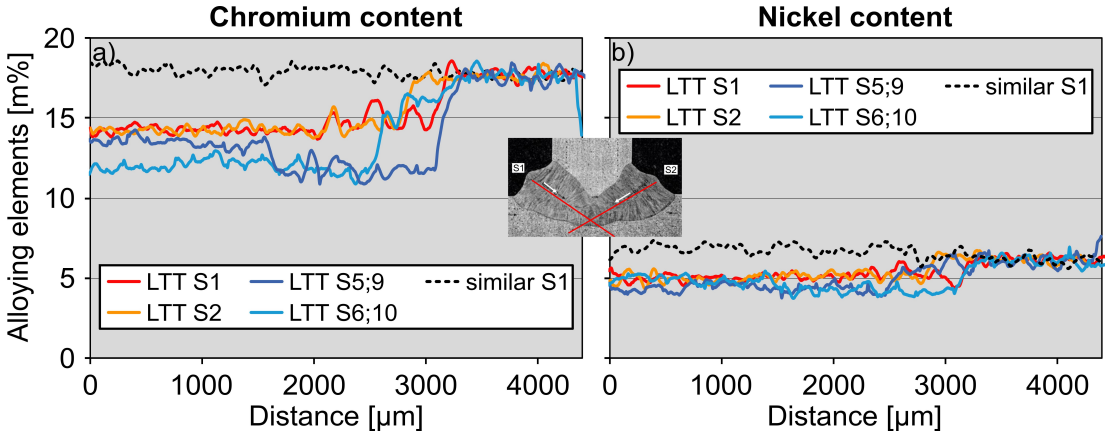


FIGURE 5 The graphs show the course of the alloy content (measured with energy dispersive x-ray spectroscopy) along the longitudinal axis of the welds. In a) the chromium content and in b) the nickel content.

BILD 5 Die Diagramme zeigen den Verlauf des Legierungsgehalts (gemessen mit energiedispersiver Röntgenspektroskopie) entlang der Längsachse der Schweißnähte. In a) der Chromgehalt und in b) der Nickelgehalt.

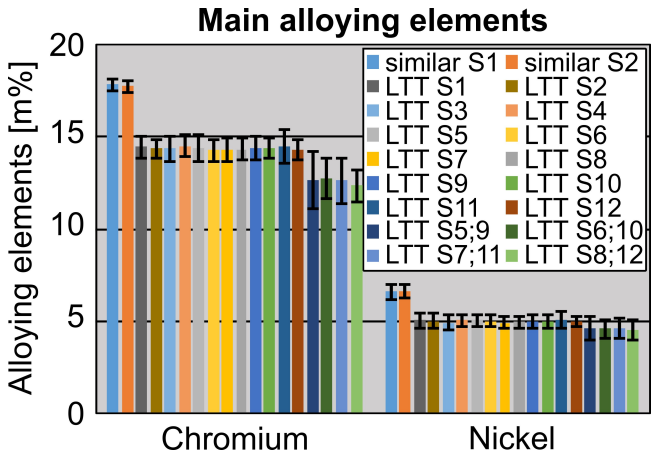


FIGURE 6 Comparison of the alloy content of chromium and nickel for all measured weld seams.

BILD 6 Vergleich des Legierungsgehalts von Chrom und Nickel für alle gemessenen Schweißnähte.

martensite start temperature (M_s) can be predicted and is calculated by equation (1) [27].

$$M_s[^\circ C] = 561 - 474^{C} - 33Mn - 17Cr - 17Ni - 21Mo \quad (1)$$

However, since the carbon content cannot be determined by energy dispersive x-ray spectroscopy, it is approximated linearly between the base material and the filler metal. Based on the chromium content of the weld seam (Cr_{WS}), the base metal (Cr_{BM}) and the filler wire (Cr_{FW}), the proportions of base metal (x_{BM}) and filler metal (x_{FW}) in the fusion zone are determined (2), (3). Using these ratios, the carbon content in the weld seam (C_{WS}) is approximated by the content of the base metal (C_{BM}) and filler wire (C_{FW}), equation (4), Table 4.

$$x_{FW} = \frac{Cr_{WS} - Cr_{BM}}{Cr_{FW} - Cr_{BM}} \quad (2)$$

$$x_{BM} = 1 - x_{FW} \quad (3)$$

$$C_{WS} = x_{FW} * C_{FW} + x_{BM} * C_{BM} \quad (4)$$

Based on these equations, the martensite start temperature can be calculated for each weld S1 to S12 and the overlap areas S5;9 to S8;12. Calculating the mean value and the standard deviation for the martensite start temperature of these two areas results in 172.17 °C ±2.29 °C for S1–S12 and 199.25 °C ±6.65 °C for S5;9 to S8;12, Table 4.

3.4 | Distortion measurement

In order to assess the influence of the low transformation temperature effect on the resulting component distortion, 5 demonstrators each set were measured with a coordinate measuring system AMS 10/10 by ZETT MESS Technik GmbH. The distortion measurements are first shown representatively on the demonstrators 003-SD and 010-LTT, Figure 7. The measurements were taken on the back side of the demonstrators, the positions on the demonstrator are plotted and the distortion is shown by the color bar. For clarity, the positions of the ribs have also been plotted. Two cross-sections (A–A and B–B) were taken in the middle of each demonstrator and plotted in separate graphs. The zero-point X0 and Y0 was placed on the bottom right corner and Z0 on the central measuring point.

The measurement of the similar demonstrator 003-SD shows an inward bulge in the sheet metal field with a

15214052, 2024, 7, Downloaded from https://onlinelibrary.wiley.com/doi/10.1002/mawe.202300164 by Rwth Aachen, Wiley Online Library on [12/12/2024]. See the Terms and Conditions (https://onlinelibrary.wiley.com/terms-and-conditions) on Wiley Online Library for rules of use; OA articles are governed by the applicable Creative Commons License

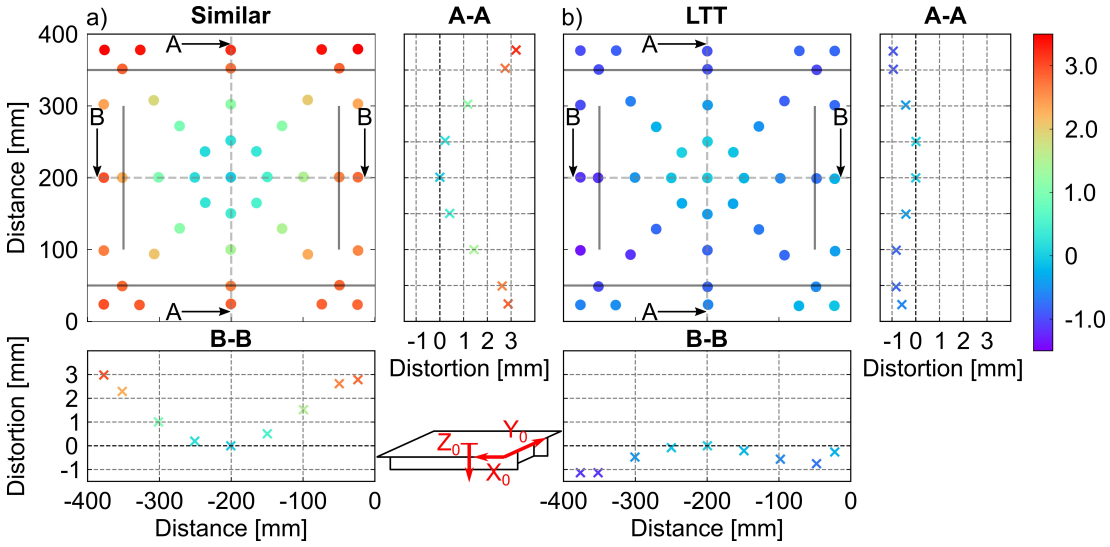


FIGURE 7 Resulting distortion of two demonstrators, subfigure a) for the similar demonstrator 003-SD and in b) for the low transformation temperature demonstrator 010-LTT.

BILD 7 Resultierender Verzug zweier Demonstratoren, Teilbild a) für den artgleichen Demonstrator 003-SD und in b) für den Niedrigtransformationstemperatur Demonstrator 010-LTT.

maximum distortion in the central measuring point, resulting in a bathtub shape, Figure 7a. A maximum distortion of 3.21 mm occurs along the line A–A and 2.98 mm along the line B–B. Comparing 003-SD with the demonstrator 010-LTT on one hand, a general reduction in welding distortion can be seen, Figure 7b. On the other hand, there is overcompensation of the welding distortion. While the similar demonstrator shows a distortion in positive z-direction, the low transformation temperature demonstrator shows a distortion in negative z-direction. The resulting shape is more reminiscent of a wave. The maximum distortion is at the middle measuring point with maximum distortion in A–A of −0.96 mm and in B–B of −1.14 mm. When comparing the two demonstrators shown, the distortion reduction of the low transformation temperature demonstrator in A–A is 70.09 % and in B–B 61.91 %.

Additionally, a structured-light 3D scanner GOM ScanCobot ATOS Q, Carl Zeiss GOM Metrology GmbH, Braunschweig, Germany, is used to measure the distortion over the whole surface. The measurement was taken on the inside between the ribs. The deviation between the computer-aided design (CAD) model and the scan of the area is displayed. A local best fit is applied to the central surface, Figure 8.

The similar demonstrator 003-SD shows a maximum deviation of 2.02 mm and −0.52 mm, which equals a difference of 2.54 mm, Figure 8a. This is smaller than the maximum distortion of the tactile measurement, which results from the different orientations of the geometry or measurements and the smaller area considered. If the edge areas behind the ribs are not considered, the two results are comparable. The deviation is off-center, meaning that the position of the maximum deviation is shifted by 6.25 mm in x-direction and 18.75 mm in y-direction from the part center. The low transformation temperature demonstrator 010-LTT results in a maximum deviation of 0.48 mm and −0.76 mm and therefore has a total range of 1.24 mm, Figure 8b. Again, the deviation distribution is off-center and the maximum is located 28.12 mm in x- and y-direction. Comparing both measurements, the maximum deviation is reduced by 51.18 %. However, the eccentricity is increased by 101.27 %.

Overall, the optical measurement confirms the results of the tactile measurement qualitatively. No further local extreme deviations are detected. With the exclusion of the area outside the ribs and segments with average scanning quality, the regarded surface is smaller than the tactile investigation. Therefore, the values of the two measurements vary only marginally and only the tactile measurements will be discussed further.

In order to compare the measurement results of all demonstrators, two section lines A–A and B–B as well as the maximum distortion value of the tactile are compared, Figure 9. All similar demonstrators measured show the formation of a bathtub shape and reach distortion values of 1.20 mm to 3.21 mm. Sample 004-SD shows the lowest distortion in both cutting directions, Figure 9a. The low transformation temperature demonstrators show significantly lower distortion values in total. The largest distortion is found in sample 013-LTT

15214052, 2024, 7, Downloaded from https://onlinelibrary.wiley.com/doi/10.1002/mawe.202300164 by Rwth Aachen, Wiley Online Library on [12/12/2024]. See the Terms and Conditions (https://onlinelibrary.wiley.com/terms-and-conditions) on Wiley Online Library for rules of use; OA articles are governed by the applicable Creative Commons License

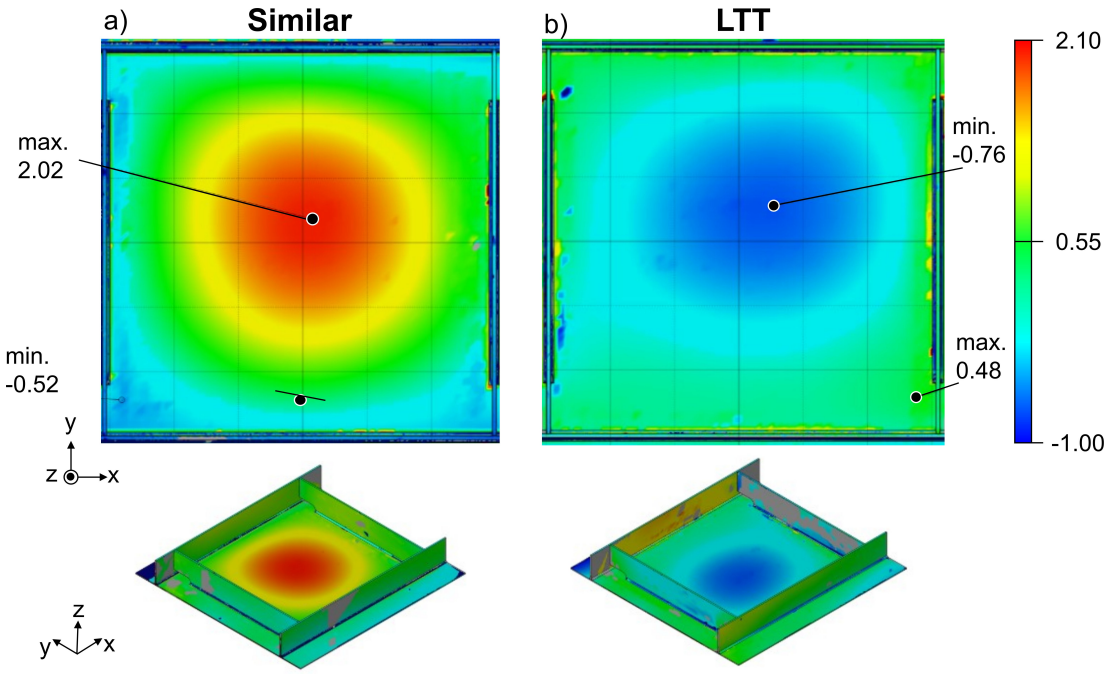


FIGURE 8 Resulting surface deviation of the demonstrator based on two samples, subfigure a) for the similar demonstrator 003-SD and in b) for the low transformation temperature demonstrator 010-LTT.

BILD 8 Resultierende Oberflächenabweichung des Demonstrators auf der Grundlage von zwei Stichproben, Teilbild a) für den artgleichen Demonstrator 003-SD und in b) für den Niedrigtransformationstemperatur Demonstrator 010-LTT.

with −1.53 mm and the smallest in sample 011-LTT with −0.65 mm, Figure 9b. The distortion is mainly in the negative z-direction with the maximum in the middle of the samples. Only the specimens 008-LTT and 013-LTT have their maximum distortion value not in the middle of the sheet metal field but related to the section A–A (x = s-200 mm) correspondingly at y = 250 mm and y = 150 mm. These do not show the formation of a wave shape but an S-shape.

However, a uniform picture emerges. The similar material demonstrators show a high distortion in positive z-direction, while the low transformation temperature demonstrators even overcompensate the distortion and show it in negative direction.

The comparison of the maximum distortion between the low transformation temperature and the similar demonstrators shows the distortion-reducing effectiveness of the low transformation temperature effect, Table 5. The maximum distortion reduction of 78.36 % is achieved in comparison of demonstrators 001-LTT with 004-SD in section B–B and the lowest reduction of −27.53 % between 013-LTT and 004-SD in section A–A. However, a mean distortion reduction of 45.51 % ±25.97 % is obtained on cut line A–A and 57.73 % ±13.98 % along cut line B–B, Table 5.

4 | DISCUSSION AND OUTLOOK

Due to the high alloy content (14.4 m% chromium and 5 m% nickel) in the welds S1–S12, a low martensite start temperature (172 °C) arises. As described in the introduction, the martensite start temperature significantly influences the formation of compressive stresses through the low transformation temperature effect. A reduction of the martensite start temperature to a lower one (T < 180 °C) leads to an incomplete martensite transformation, as the martensite finish temperature falls below room temperature. The literature indicate that an incomplete martensite transformation leads to reduced dilatation during phase transformation, thus reducing the formation of compressive stresses [12,15,28]. Furthermore, literature shows an optimum at about 180 °C–200 °C [16,28]. Seams S1–S12 therefore appear to already have a lower martensite start temperature than is reasonable for the maximum introduction of compressive stresses into the weld. Furthermore, it is possible that the martensite finish temperature has already fallen below room temperature and that portions of austenite therefore remain in the weld. Whether this is the case and what influence a certain proportion of austenite has on the behavior of the weld should be investigated further.

A main requirement for rail vehicles made of stainless chromium-nickel steels is corrosion resistance. To

15214052, 2024, 7, Downloaded from https://onlinelibrary.wiley.com/doi/10.1002/mawe.202300164 by Rwth Aachen, Wiley Online Library on [12/12/2024]. See the Terms and Conditions (https://onlinelibrary.wiley.com/terms-and-conditions) on Wiley Online Library for rules of use; OA articles are governed by the applicable Creative Commons License

TABLE 5 Reduction of distortion of the low transformation temperature demonstrators along the cutting lines A–A and B–B compared to the similar demonstrators.

TABELLE 5 Verringerung des Verzuges der Niedrigtransformationstemperatur-Demonstratoren entlang der Schnittlinien A–A und B–B im Vergleich zu den artgleichen Demonstratoren.

Reduction of distortion A–A [%]							
	003-SD	**004-SD**	**005-SD**	**006-SD**	**007-SD**		**[%]**
008-LTT	60.59	−5.86	37.06	55.54	50.00	Maximum	76.32
010-LTT	70.09	19.67	52.24	66.26	62.06	Minimum	−27.53
011-LTT	76.32	36.40	62.19	73.29	69.96	Mean	45.51
012-LTT	63.08	0.84	41.04	58.35	53.16	Standard deviation	25.97
013-LTT	52.52	−27.53	24.18	46.43	39.76		
Reduction of distortion B–B [%]							
	003-SD	**004-SD**	**005-SD**	**006-SD**	**007-SD**		**[%]**
008-LTT	70.47	40.94	60.18	67.53	63.64	Maximum	78.36
010-LTT	61.91	23.83	48.64	58.12	53.10	Minimum	23.83
011-LTT	78.36	56.71	70.81	76.20	73.35	Mean	57.73
012-LTT	64.09	28.19	51.58	60.52	55.79	Standard deviation	13.98
013-LTT	66,95	33,89	55,43	63,65	59,30		

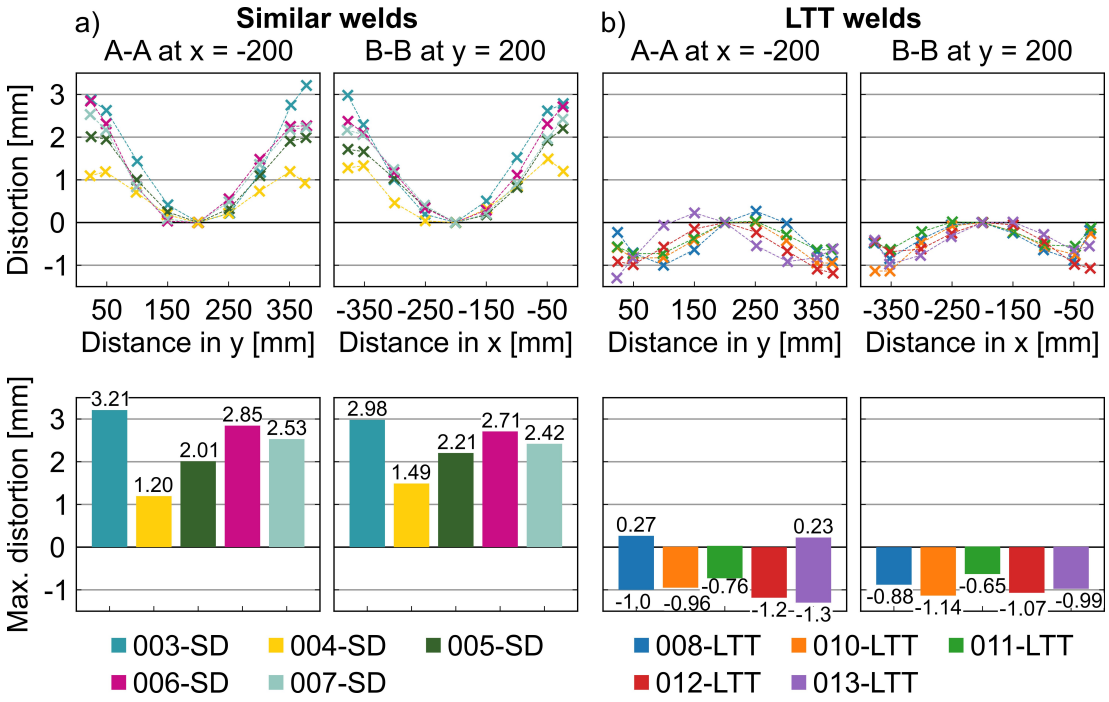


FIGURE 9 Distortion of all welded demonstrators along section lines A–A and B–B. In a) for the similar welds and in b) for the low transformation temperature welds.

BILD 9 Verzug aller geschweißten Demonstratoren entlang der Schnittlinien A–A und B–B. In a) für die artgleichen Schweißnähte und in b) für die Niedrigtransformationstemperatur Schweißnähte.

protect the weld from corrosive attack, the same alloy content as in the base metal is aimed for, as can also be seen in the example of the similar joint made of 1.4318 + G19 9. Reduced corrosion resistance for both kind of seams S1–S12 (approx. 14.4 m% Cr, 5.0 m% Ni) and S5;9 to S8;12 (approx. 12.7 m% Cr, 4,6 m% Ni) can be expected, with the low alloy content of seams S5;9 to S8;12 appearing most critical. However, for all weld seams the critical value of 12 m% chromium content is retained. Further investigations will be carried out in the

15214052, 2024, 7, Downloaded from https://onlinelibrary.wiley.com/doi/10.1002/mawe.202300164 by Rwth Aachen, Wiley Online Library on [12/12/2024]. See the Terms and Conditions (https://onlinelibrary.wiley.com/terms-and-conditions) on Wiley Online Library for rules of use; OA articles are governed by the applicable Creative Commons License

future to determine the extent of the weakening of the corrosion resistance.

In joints of the similar type, the welding process causes tensile stresses during cooling, which lead to contraction in the top of the welds. From the theory, the weld distortion in a fillet weld will occur mainly in the form of angular distortion, pulling the belt plate upwards [7]. For the similar demonstrators, the plate field bulges inward, thus between the welded-on webs, and a component distortion of up to 3.21 mm occurs, Figures 7–9 789.

If compressive stresses are induced into the weld by an low transformation temperature effect, then these counteract the inward buckling caused by the tensile stresses. With an increase in the applied compressive stresses, the inward buckling of the sheet metal field should first be reduced until a flat state is achieved and with a further increase, the sheet metal field should then buckle outwards. The demonstrators with low transformation temperature effect show an outward bulging sheet metal field (up to 1.3 mm in specimen 013-LTT), which therefore represents an overcompensation. Based on this consideration, the achieved low transformation temperature effect seems to have too strong distortion-reducing effect for the welding task. One way to counteract this is to adapt the low transformation temperature effect to the requirements of the welding task. The most obvious way to do this is to vary the alloy content in the welds. The aim should be to introduce lower compressive stresses into the process. Either by increasing the martensite start temperature (lower alloy content) and thus further shrinkage occurs after the completed martensite transformation or by further reducing the martensite start temperature. A further reduction results in an incomplete martensite transformation and thus a smaller volume available for the introduction of compressive stresses. However, in terms of corrosion resistance, increasing the alloy content seems to be the obvious option. Accordingly, in addition to investigations on corrosion resistance, studies on the microstructure that develops and the influence of different alloy compositions will follow in further work.

In conclusion, it can be stated that:

- Using a commercially available unalloyed filler wire G4Si1, the alloy content in the weld seams S1 to S12 can be homogeneously reduced to 14.4 m% chromium and 5.0 m% nickel. For the seams in the overlap area S5;9 and S8:12, 12.7 m% chromium and 4.6 m% nickel was achieved.
- In the low transformation temperature demonstrators, the hardness increases from 361 HV0.2 to 383 HV0.2. Together with the reduced alloy content, this indicates a potentially martensitic weld seam.
- The measurements of the welding distortion using both the coordinate measuring system and the GOM scanners show a significant reduction in distortion in the demonstrators with the low transformation temperature effect. The maximum distortion reduction is 78 %, whereby the mean values in both directions A–A and B–B are 45.5 % and 57.7 % respectively.
- The similar reference demonstrators bulge inwards, whereas the low transformation temperature demonstrators bulge outwards. This indicates an overcompensation of the resulting welding distortion due to the low transformation temperature effect.

ACKNOWLEDGEMENTS

Open Access funding enabled and organized by Projekt DEAL.

CONFLICT OF INTERESTS

The authors declare no financial or commercial conflict of interest.

DATA AVAILABILITY STATEMENT

The data that support the findings of this study are available from the corresponding author upon reasonable request.

ORCID

M. Gamerdinger http://orcid.org/0000-0003-3992-6559
F. Akyel http://orcid.org/0000-0002-2807-8745
C. Kahve http://orcid.org/0000-0002-0340-8437
D. C. Fritsche http://orcid.org/0000-0001-9225-1285
U. Reisgen http://orcid.org/0000-0003-4920-2351

REFERENCES

1. T. Nitschke-Pagel, H. Wohlfahrt, *MSF* **2002**, *404–407*, 215.
2. U. Zerbst, *Weld. World* **2020**, *64*, 151.
3. J. C. Lippold, *Welding Metallurgy and Weldability*, John Wiley & Sons, Inc., Hoboken, New Jersey, **2015**.
4. P. J. Withers, H. Bhadeshia, *Mater. Sci. Technol.* **2001**, *17*, 366.
5. Y. Mikami, Y. Morikage, M. Mochizuki, M. Toyoda, *Sci. Technol. Weld. Joining* **2009**, *14*, 97.
6. P. Michaleris, in *Encyclopedia of Thermal Stresses* (Ed.: R. B. Hetnarski), Springer Netherlands, Dordrecht, **2014**.
7. K. Masubuchi, *Analysis of welded structures*, Pergamon Press, Oxford, **1980**.
8. Y.-P. Yang, *WJ* **2021**, *100*, 193.
9. J. Sun, K. Dilger, *J. Adv. Joining Processes* **2023**, *8*, 100157.
10. J. Wang, X. Zhou, B. Yi, *CIRP J. Manuf. Sci. Technol.* **2022**, *37*, 278.
11. J. Tomków, K. Sobota, S. Krajewski, *FU Mech Eng* **2020**, *18*, 611.
12. S. A. Hosseini, K. Gheisari, H. Moshayedi, F. Warchomicka, N. Enzinger, *Sci. Technol. Weld. Joining* **2020**, *25*, 243.

15214052, 2024, 7, Downloaded from https://onlinelibrary.wiley.com/doi/10.1002/mawe.202300164 by Rwth Aachen, Wiley Online Library on [12/12/2024]. See the Terms and Conditions (https://onlinelibrary.wiley.com/terms-and-conditions) on Wiley Online Library for rules of use; OA articles are governed by the applicable Creative Commons License

13. S. Wu, D. Wang, Z. Zhang, C. Li, X. Liu, X. Meng, Z. Feng, X. Di, *Sci. Technol. Weld. Joining* **2019**, *24*, 112.
14. A. Ohta, O. Watanabe, K. Matsuoka, C. Siga, S. Nishijima, Y. Maeda, N. Suzuki, T. Kubo, *Weld. World* **1999**, *43*, 38.
15. S. A. Hosseini, K. Gheisari, H. Moshayedi, M. R. Ahmadi, F. Warchomicka, N. Enzinger, *Weld. World* **2021**, *65*, 807.
16. Z. Feng, N. Ma, K. Hiraoka, Y. Komizo, S. Kano, M. Nagami, *Sci. Technol. Weld. Joining* **2023**, *28*, 305.
17. J. A. Francis, H. J. Stone, S. Kundu, R. B. Rogge, H. K. D. H. Bhadeshia, P. J. Withers, L. Karlsson, *Transformation Temperatures and Welding Residual Stresses in Ferritic Steels.* in: Lidbury D (ed) Proceedings of the ASME Pressure Vessels and Piping Conference – 2007: Presented at 2007 ASME Pressure Vessels and Piping Conference, July 22–26, 2007, San Antonio, Texas, USA. ASME, New York, NY, **2008**, 949.
18. E. Harati, L. Karlsson, L.-E. Svensson, K. Dalaei, *Int. J. Fatigue* **2017**, *97*, 39.
19. A. Kromm, V. van der Mee, T. Kannengiesser, B. Kalfsbeek, *Weld. World* **2015**, *59*, 413.
20. F. Akyel, M. Gamerdinger, S. Olschok, U. Reisgen, A. Schwedt, J. Mayer, *Metals* **2022**, *12*, 911.
21. F. Akyel, M. Gamerdinger, S. Olschok, U. Reisgen, A. Schwedt, J. Mayer, *J. Adv. Joining Processes* **2022**, *5*, 100081.
22. F. Akyel, S. Olschok, U. Reisgen, *Weld. World* **2021**, *65*, 23.
23. J. M. J. McDill, A. S. Oddy, J. A. Goldak, S. Bennison, *J STRAIN AN* **1990**, *25*, 51.
24. DIN Deutsches Institut für Normung e. V., Zerstörende Prüfung von Schweißverbindungen an metallischen Werkstoffen – Makroskopische und mikroskopische Untersuchungen von Schweißnähten (ISO 17639 : 2022), 2022.
25. DIN Deutsches Institut für Normung e. V., Zerstörende Prüfung von Schweißverbindungen an metallischen Werkstoffen – Härteprüfung –Teil 2: Mikrohärteprüfung an Schweißverbindungen (ISO 9015–2 : 2016), 2016.
26. M. Gamerdinger, F. Akyel, S. Olschok, U. Reisgen, *Procedia CIRP* **2022**, *111*, 420.
27. W. Steven, A. G. Haynes, *J. Iron Steel Inst. London* **1956**, *183*, 349.
28. W. Wang, L. Huo, Y. Zhang, D. Wang, H. Jing, *J. Mater. Sci. Technol.* **2002**, *18*, 527.

How to cite this article: M. Gamerdinger, F. Akyel, S. Olschok, C. Kahve, D. C. Fritsche, U. Elliesen, C. Hopmann, U. Reisgen, *Materialwiss. Werkstofftech.* **2024**, *55*, e202300164.
https://doi.org/10.1002/mawe.202300164

15214052, 2024, 7, Downloaded from https://onlinelibrary.wiley.com/doi/10.1002/mawe.202300164 by Rwth Aachen, Wiley Online Library on [12/12/2024]. See the Terms and Conditions (https://onlinelibrary.wiley.com/terms-and-conditions) on Wiley Online Library for rules of use; OA articles are governed by the applicable Creative Commons License